Engenharia Agrícola

ISSN: 1809-4430 (on-line)

www.engenhariaagricola.org.br

Scientific Paper
Doi: http://dx.doi.org/10.1590/1809-4430-Eng.Agric.v43n4e20220207/2023

NUMERICAL SIMULATION AND EXPERIMENTAL ANALYSIS OF SPRAY FIELD OF IMPINGEMENT NOZZLE

Fulong Dong[1], Wenjian He[2*], Hongping Zhou[3]

[2*]Corresponding author. Information Department, Beijing City University/Beijing, China.
Email: hwj6666@163.com | ORCID ID: https://orcid.org/0000-0001-9822-5037

KEYWORDS

impingement nozzle, numerical simulation, spray field, particle size uniformity, droplet spectrum.

ABSTRACT

The shape of a spray droplet from a flat-fan nozzle in the plant protection sector is similar to a 'U shape', the middle particle size being small but the diameter of both sides being too large. So, flat-fan nozzles have the defects of wide droplet size and poor uniformity of droplet size. This paper simulates and tests the impingement nozzle, based on the coupling effect of the jet and impinging stream, so as to improve the droplet size uniformity and droplet spectrum. After jet impingement, it was found that the droplet size of the spray fan surface of the impingement nozzle showed the characteristics of large, uniform and smaller sides. This was beneficial in solving the uneven distribution of droplet size distribution in the field operation of the sprayer. The droplet distribution of the impingement nozzle is more concentrated, forming a narrow droplet spectrum. The experimental results are in good agreement with the results of numerical simulations and theoretical analysis. The impingement nozzle solves the shortcomings of wider fan droplets and smaller particle size uniformity, and provides feasible technical support for developing intelligent precision spray equipment.

INTRODUCTION

As an important tool for protecting agricultural, forestry, fruit and livestock production, plant protection machinery plays an important role in protecting stable and high crop yields (Dong et al., 2019). As one of the important components of the spraying system of plant protection machinery, the performance of the nozzle is related to the reliability and economy of the whole plant protection machinery and the operation of the whole system; it is also a key element in the improvement of spraying technology (Wang, 2019; Dong & Zhou, 2018). Nozzle jet spray atomisation is a multi-phase flow stochastic process with gas-liquid phase interaction, and there is no universally applicable relevant theory for the atomisation mechanism. Researchers at home and abroad have conducted a lot of experimental and theoretical research in this area (He, 2019; Song et al., 2017; Salcedo et al., 2020). Lü et al. (2007) studied the spatial distribution of droplet size and motion of a standard fan nozzle and found that the droplet particle size distribution showed a concave ellipsoidal distribution, with a small middle edge and a large edge, when gradually moving away from the nozzle terminal outlet section. The droplet velocity in the axial direction was a hill-shaped distribution with a large middle edge. Zheng et al. (2015) used the CLSVOF method to study the impact angle of the collision nozzle on the atomisation. It was found that the fragmentation length of the liquid film decreases as the impact angle increases, while the surface wave amplitude and fragmentation of the liquid film also increases. The velocity difference at the impact position plays a key role in the fragmentation and surface wave amplitude of the liquid film. Fei et al. (2015) studied the droplet motion process and particle size distribution characteristics of jet impingement nozzle atomisation under atmospheric conditions. The analysis of the process of impingement jet atomisation and liquid film fragmentation into droplets found that the velocity of atomised droplets in the radial velocity component (relative to the origin as the centre of symmetry) away from the origin increases. The radial velocity distribution and the initial atomisation stage droplet size distribution was the opposite.

[1] College of Mechanical Engineering, Anhui Science and Technology University/Fengyang, China.
[3] College of Mechanical and Electronic Engineering, Nanjing Forestry University/Nanjing,China.

Area Editor: João Paulo Arantes Rodrigues da Cunha
Received in: 11-13-2022
Accepted in: 10-2-2023

The hedge nozzle is a fan-impact nozzle based on the coupling effect of impinging the flow and the jet, which has the characteristics of a narrow droplet spectrum and better particle size uniformity, relative to the fan nozzle (Dong et al., 2018). The analysis of the fluid flow field in the impinging region outside the nozzle, using Fluent software, is of great significance to the spray mechanism and nozzle structure optimisation.

Hedge nozzle working principle and geometric modelling

Working principle

Many researchers (Zhang et al., 2022; Cai et al., 2022) found that the impact of the two jets can make the droplet particle size distribution narrower, homogenising the droplet group particle size; the more intense the impact, the more obvious the particle size homogenisation effect. As shown in Figure 1, the hedge nozzle has two jets from the terminal outlet at a certain angle, which hit each other at the impact surface, and the impact makes the droplet particle size distribution narrower and homogenises the droplet group. This improves the current fan spray as the droplet spectrum is wider but the particle size uniformity is poor.

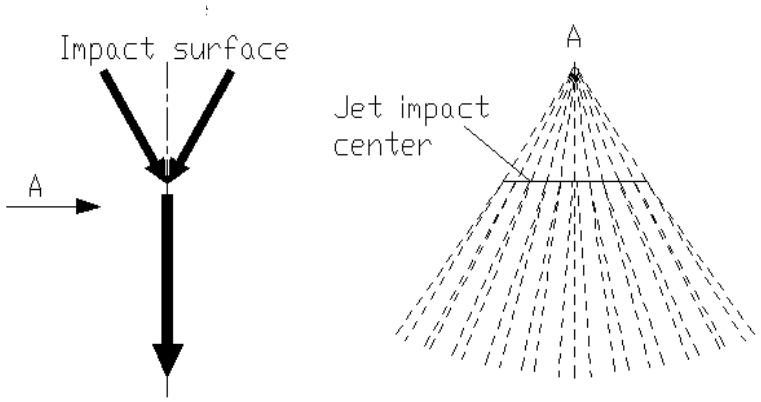

FIGURE 1. Schematic diagram of impinging jet.

Geometric modelling

Figure 2(a) shows part of the experimental test set-up: the outlet orifice diameter was 1 mm, the distance between the two outlets was 7 mm, the notch angle of the hedge nozzle was 30° (two jets impacting before the spray surface) and the vertical impact surface angle was 15°. The internal fluid region of the model nozzle is shown in Figure 2(b) and the black area in Figure 2(c) shows the fluid domain inside the hedge nozzle.

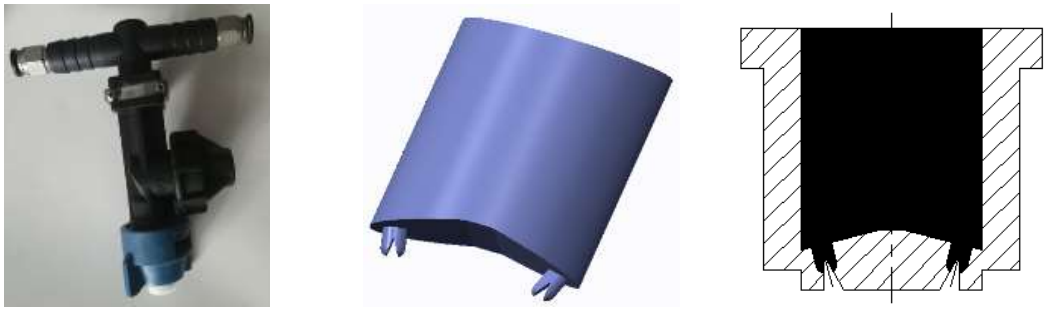

(a) (b) (c)

FIGURE 2. Geometric model.

According to the model of the hedge nozzle geometry, the model was meshed using the ANSYS mesh pre-processing software 'ICEM CFD' (Gu et al., 2015), as shown in Figure 3. In order to obtain more accurate calculation results, the spray field mesh was divided into three parts in the back section of the spray nozzle terminal orifice outlet. According to the actual situation, and taking into account the dense nozzle jet impact region, jet impact and droplet fragmentation occurs in this region. The second part of the mesh for local grid encryption processing (mm), the first part of the grid second dense (mm), and the third part of the grid is the coarsest (mm). In order to facilitate the calculation and to obtain the results, a hexahedral-structured grid topology was used, with a mesh count of 695557.

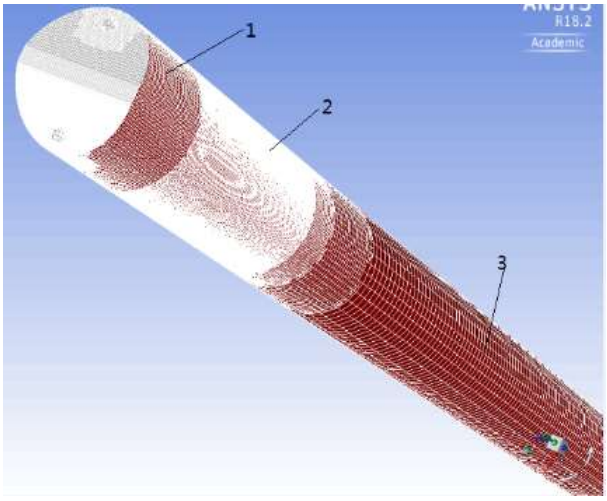

FIGURE 3. Meshing of the model.

Model and parameter settings

Mathematical model

VOF model

A traditional fan nozzle only has one jet, and the 'DPM' discrete phase processing method is usually used for simulation; it is believed that the spray droplets will be formed directly at the outlet, allowing visual simulation of the spray nozzle atomisation process (Wang et al., 2022). The hedge nozzle originated from the jet impact, and the outlet cannot be used in this spray mode model. The water flow just comes out of the nozzle's terminal orifice outlet and can be considered to be jet-like. This then collides with the impact surface or impact centre near the outlet, to form many fine droplets. The use of VOF two-phase flow model processing can better fit the actual situation. However, the VOF model can only show the velocity distribution and shape of the spray field, it cannot obtain the spray nozzle atomisation process condition. The model uses volume fraction to characterise the volume percentage of the second phase fluid in the computational grid cell. In the calculation, when F=0, it is considered that the grid is all gas; when F=1, it is considered that the grid is all liquid and, when 0<F<1, it is considered that the grid is a gas-liquid mixture.

$$\frac{\partial F}{\partial t}+\vec{v}\cdot\nabla F=0 \tag{1}$$

In the equation, time, Speed vector, Fluid Density, Fluid viscosity. In the gas-liquid mixing zone, fluid density and viscosity can be expressed as $\rho=(1-F)\rho_g+F\rho_l$ and $\mu=(1-F)\mu_g+F\mu_l$, respectively.

Gas-liquid phase control equations

In the study of the flow field process outside the hedge nozzle, the gas and liquid are considered to be incompressible fluids, and the controlling equations have a mass and momentum conservation equation. The mass conservation equation is:

$$\frac{\partial\overline{\rho}}{\partial t}+\frac{\partial(\overline{\rho}v_i)}{\partial x_i}=0 \tag{2}$$

The conservation of momentum equation is given by:

$$\frac{\partial(\overline{\rho}\cdot\overline{u}_i)}{\partial t}+\frac{\partial(\overline{\rho}\cdot\overline{u}_j\overline{u}_i)}{\partial x_j}=-\frac{\partial\overline{p}}{\partial x_i}+\overline{\mu}\nabla^2\overline{u}_i+\frac{\overline{\mu}}{3}\frac{\partial^2\overline{u}_j}{\partial x_j\partial x_i}+\overline{S} \tag{3}$$

In the equation, $\overline{\rho}$ is density, $\overline{\mu}$ is power viscosity, $\overline{u}_i$ is the speed vector, and $\overline{S}$ is a generalised source term of the momentum equation.

Turbulence model

A model which achieved (Realizable) $k-\varepsilon$ was chosen for the study.

The turbulent kinetic energy (k) equation is:

$$\frac{\partial(\rho k)}{\partial t}+\frac{\partial(\rho kU)}{\partial x_i}=\frac{\partial}{\partial x_j}[(\mu+\frac{\mu_t}{\sigma_k})\frac{\partial k}{\partial x_j}]+G_k+G_b-\rho\varepsilon-Y_M \tag{4}$$

The turbulence dissipation rate (ε) equation is:

$$\frac{\partial(\rho\varepsilon)}{\partial t}+\frac{\partial(\rho\varepsilon u_i)}{\partial x_i}=\frac{\partial}{\partial x_j}[(\mu+\frac{\mu_t}{\sigma_\varepsilon})\frac{\partial\varepsilon}{\partial x_j}]+\rho C_1E\varepsilon-C_{2\varepsilon}\rho\frac{\varepsilon^2}{k+\sqrt{v\varepsilon}}+\frac{C_{1\varepsilon}\varepsilon}{k}C_{3\varepsilon}G_b \tag{5}$$

In the equation, $C_1=\max(0.43,\eta/(\eta+5))$, $\eta=(2E_{ij}E_{ij})^{1/2}k/\varepsilon$, and the turbulent viscosity coefficient $\mu_t=\rho C_\mu k^2/\varepsilon$. G_k is the generation term of turbulent kinetic energy k due to the mean velocity gradient, G_b is the generation term of turbulent kinetic energy k due to buoyancy, Y_M is the contribution of the pulsation expansion to the total dissipation rate in compressible turbulent flows, (G_μ, $G_{1\varepsilon}$, $G_{2\varepsilon}$) and $G_{3\varepsilon}$ indicates the empirical constant. σ_k is the Prandtl number corresponding to turbulent kinetic energy, and σ_ε is the Prandtl number corresponding to the dissipation rate. In FLUENT, $G_{\varepsilon1}=1.44$, $G_{2\varepsilon}=1.9$, $G_{3\varepsilon}=0.09$, $\sigma_k=1.0$, and $\sigma_\varepsilon=1.2$.

Boundary condition setting

The nozzle's external flow field was modelled using the following basic assumptions: nozzle external flow is a two-stream transient flow problem, the fluid and air are an incompressible Newtonian fluid, the physical properties are constant and there are no chemical reactions, and the effect of gravity on atomisation is ignored without considering convective heat transfer.

The experiment investigated the effect of three different spray pressures on the spray condition of the nozzle, setting the nozzle inlet boundary in the boundary definition as the pressure-inlet during the simulation; the pressure-outlet was connected to the external atmospheric pressure. Therefore, it is necessary to know the external atmospheric pressure. The velocity at the inlet of the external flow field (i.e. the pressure-outlet of the internal flow field) was obtained from the calculation of the internal flow field and the data are the same as in the internal flow field simulation. The nozzle inlet in the boundary condition was the nozzle inlet during the internal flow field simulation; the inlet pressure parameters were set to 0.3, 0.5 and 0.7 MPa, respectively. Air pressure was the relative static pressure at 0.0 MPa (i.e. atmospheric pressure). Air density was set at 1.225 kg/m3 and viscosity was 1.789 kg/(ms). Using no-slip boundary conditions, the jet medium was water with a density of 998 kg/m^3 and a viscosity of 0.001 kg/(ms); a time step of 1e-5 was used in the calculations.

Simulation results and analysis

Cloud analysis of impact models

The impact model clouds of the hedge nozzles at spraying pressures of 0.3, 0.5 and 0.7 MPa are shown in Figure 4. It is found that the droplet particle size, after the impact of the two jets, becomes smaller and more uniform as the spray application pressure increases, which is consistent with the conclusion that the stronger the impact is, the more favourable the jet atomisation. As reflected in Figure 4, it can be seen that the splitting and uniformity of the liquid stream cluster has more obvious changes with increasing pressure; Figure 4(c) shows the best uniformity of the hedge nozzle atomisation particle size at 0.7 MPa.

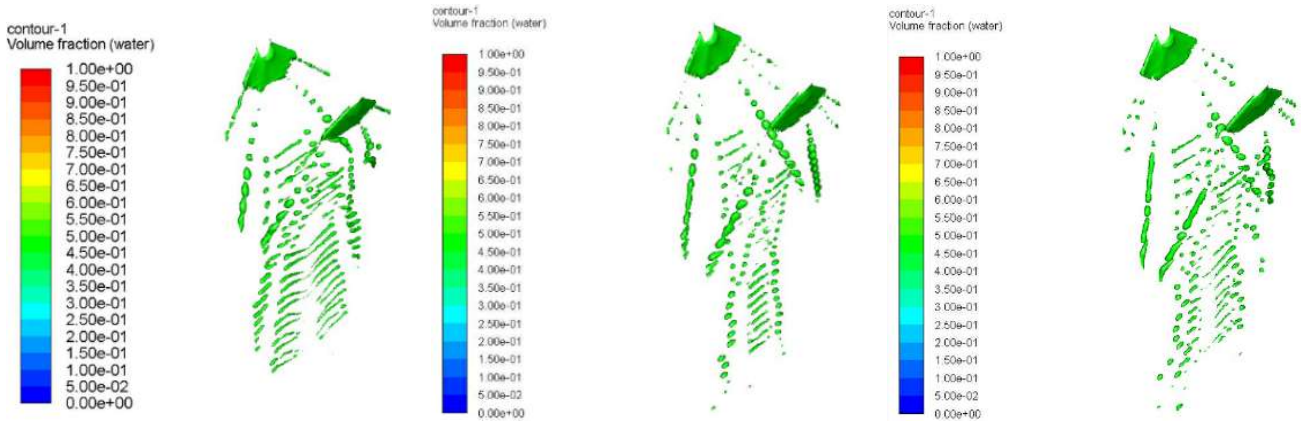

(a) 0.3 MPa (b) 0.5 MPa (c) 0.7 MPa

FIGURE 4. Impact model cloud picture.

Distribution analysis of droplet velocity

Lu Xiaolan, Liu Qiusheng and many other scholars found that droplet velocity plays a significant role in the spray atomisation process. The commonly used fan nozzle droplet particle size in the spray sector is not the same, in the same height horizontal direction presents the middle of the droplet diameter is small to gradually increase on both sides, while the measured droplet velocity in the axial direction shows a trend of gradually decreasing in the middle and at both sides. This indicates that there is a certain relationship between droplet velocity and droplet diameter and analysis and speculation suggests that droplets with similar velocities in the axial direction, at the same height and horizontal direction, will tend to have the same droplet size.

For spraying pressures of 0.3, 0.5 and 0.7 MPa, the test points were defined using FLUENT software. The coordinates of the points were entered and calculated, and the resulting data files were processed to derive the velocities in the x, y and z directions for each test point, i.e. the velocity components of the droplets in each direction, as shown in Figure 5.

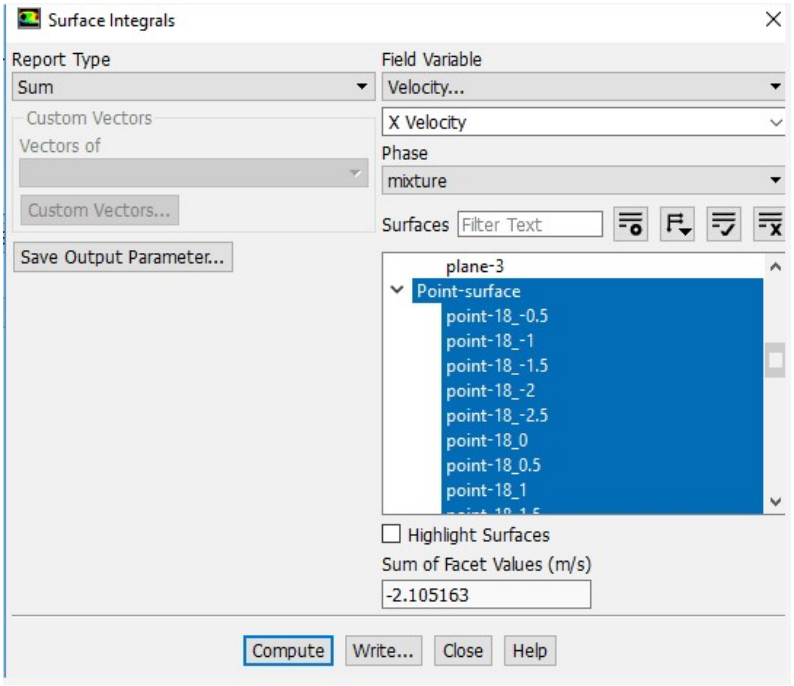

FIGURE 5. Droplet velocity output.

The specific test point location of the hedging nozzle is shown in Figure 6. Figure 6(c) shows the geometric model of the hedging nozzle body at the bottom end of the centre of the circle: the vertical direction represents the z-axis, the horizontal direction of the spray sector is the x-axis, perpendicular to the spray sector direction for the y-axis, and x, y and z are the three axes of direction in line with the right-hand spiral relationship. By testing the velocity components of the droplet velocity in the x, y and z directions in the XOZ plane, and at vertical heights of 18, 23 and 28 mm from the origin, the test point locations are shown in Figures 6(a) and 6(b). The measured velocity components of the droplet velocity in the x, y and z directions are shown in Tables 1, 2 and 3, for each test point symmetrical to the left and right, i.e. the -2.0, -1.5, -1.0, -0.5, 0.0, 0.5, 1.0, 1.5 and 2.0 mm positions measured from the centreline position (i.e. z-axis) of the spray sector.

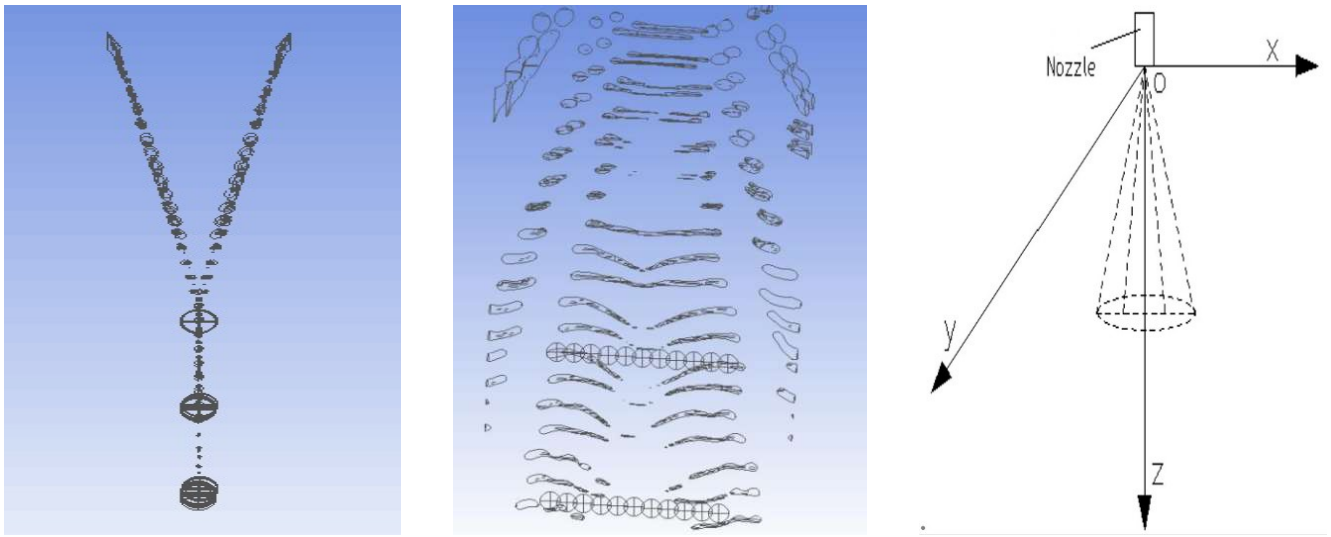

(a) (b) (c)

FIGURE 6. Test location diagram.

From Table 1, it can be seen that, in the vertical direction (i.e. the height or z-direction), at a spraying pressure of 0.3 MPa, the droplet velocity component at 18 mm is smaller than that at 23 mm (at the point -0.5, 0.0, 0.5). Because the droplets are closer to the impact centre, the droplets may be more dense and not yet fully atomised. The velocity components of droplets at different pressures in the z-direction, i.e. vertical height, are close to those in the horizontal direction (e.g. at 0.5 Mpa pressure). At a horizontal height of 23 mm, the velocity components of droplets are between 70.33 and 73.70 m/s. As the spraying pressure increases, the droplet velocity increases accordingly, and at the outlet away from the nozzle, the velocity decreases. For example, at 0 mm on the z-axis, and with a spray pressure of 0.5 Mpa (at 18, 23 and 28 mm), the speeds are 74.821, 73.701, and 72.960 m/s,

respectively. At a spray pressure of 0.7 Mpa, at 18, 23 and 28 mm, the speeds are 94.108, 93.452, and 90.698 m/s, respectively. As the droplet moves away from the nozzle's terminal outlet, the droplet velocity will be reduced, mainly because of the role of air disturbance/resistance. As the hedge nozzle after impact droplet velocity in the z-axis direction of the velocity component is similar, then the same height in the spray field in the horizontal direction of the droplet diameter should tend to the same trend (i.e. uniform particle size).

As can be seen from Table 2, in the left and right direction (i.e. the x-direction), and for the horizontal direction of the same height at different pressures, the droplet velocity in the x-axis component shows a trend of gradually increasing from the middle towards both sides. With an increase in pressure, the droplet velocity component also increases but in a position closer to the central axis (the z-axis), especially near the z-axis line. The droplet velocity component changes irregularly and the value is small; the gradual increase in the droplet velocity component near both sides of the edge is conducive to the formation of the spray fan surface.

From Table 3, it can be seen that in the y direction, the velocity components of droplets at the same height in the horizontal direction, under different pressures, are close to 0, with small values and irregular state motion. It can be considered that the droplets are basically unaffected in the front-to-back direction.

TABLE 1. Fog droplet velocity component in vertical direction.

Pressure (MPa)	z (mm)	Fog droplet velocity component at test point position (mm)（m/s）								
		-2.0	-1.5	-1.0	-0.5	0.0	0.5	1.0	1.5	2.0
0.3	18	58.36	58.06	56.71	56.00	55.94	55.61	57.28	58.49	58.10
	23	57.75	56.45	54.11	57.05	57.28	57.40	55.15	57.04	58.08
	28	57.72	52.63	55.07	53.69	53.22	54.67	51.34	56.68	57.51
0.5	18	75.49	71.31	72.63	74.07	74.82	74.07	72.55	72.01	74.20
	23	72.46	70.33	72.16	73.43	73.70	71.83	72.14	71.21	72.93
	28	66.63	71.44	71.95	72.60	72.96	70.73	71.12	71.15	63.12
0.7	18	92.20	93.03	93.35	94.04	94.11	94.60	94.43	93.99	92.95
	23	93.74	93.08	93.18	93.11	93.45	93.32	92.32	91.29	93.82
	28	92.17	92.49	92.50	90.86	90.70	87.30	89.91	90.57	91.36

TABLE 2. Fog droplet velocity component in horizontal direction.

Pressure (MPa)	x (mm)	Fog droplet velocity component at test point position (mm)（m/s）								
		-2.0	-1.5	-1.0	-0.5	0.0	0.5	1.0	1.5	2.0
0.3	18	-7.90	-6.66	-4.99	-2.94	0.11	3.49	4.86	5.23	7.64
	23	-6.34	-5.10	-1.82	-1.18	-0.23	0.24	2.51	5.21	5.94
	28	-5.63	-4.86	-4.32	-3.45	-1.99	1.74	3.34	4.35	5.36
0.5	18	-6.81	-5.19	-3.92	-2.21	0.96	5.52	5.13	3.95	8.29
	23	-6.15	-3.17	-2.31	-1.03	-0.42	0.24	2.23	3.72	8.06
	28	-5.46	-4.47	-3.87	-3.16	-2.28	0.91	3.47	5.63	7.02
0.7	18	-12.93	-8.95	-6.79	-3.46	-0.74	3.63	7.16	8.87	12.43
	23	-8.91	-7.13	-5.63	-2.90	-1.51	1.17	3.35	4.01	9.02
	28	-6.83	-6.54	-6.23	-3.60	-2.08	0.77	2.67	3.83	5.21

TABLE 3. Fog droplet velocity component in front and rear directions.

Pressure (MPa)	y (mm)	Fog droplet velocity component at test point position (mm)（m/s）								
		-2.0	-1.5	-1.0	-0.5	0.0	0.5	1.0	1.5	2.0
0.3	18	-0.084	-0.263	-0.219	-0.052	0.293	-0.119	-0.278	-0.075	-0.062
	23	-0.065	0.036	-0.024	-0.072	-0.050	-0.020	0.111	-0.055	-0.039
	28	0.004	-0.253	-0.234	-0.281	-0.327	-0.248	-0.279	-0.160	-0.061
0.5	18	-0.671	-0.001	-0.144	-0.229	-0.252	-0.171	-0.022	-0.101	-0.226
	23	0.005	0.182	-0.005	-0.025	-0.015	-0.048	-0.033	-0.071	-0.246
	28	-0.092	-0.039	-0.051	-0.041	-0.118	-0.012	-0.205	-0.191	-0.063
0.7	18	-0.143	-0.027	-0.088	-0.157	-0.246	-0.291	-0.116	0.006	0.098
	23	-0.006	-0.031	-0.170	0.084	-0.041	-0.308	-0.055	-0.321	-0.143
	28	0.077	0.048	0.020	-0.069	-0.187	-0.213	-0.013	-0.006	0.010

In summary, after the two jets of the hedging nozzle impacted, the velocity component of the droplet velocity is similar in the x-axis direction, characterised by the same height direction in the spray field, and the droplet diameter should tend to the same trend (i.e. uniform particle size). The velocity of the droplets at the same height in the horizontal direction on the x-axis, shows a trend of being small in the middle to gradually increasing on both sides; the gradual increase of the velocity component of the droplets near both sides of the edge facilitates the formation of a spray fan. For the traditional fan nozzle measured in the direction of the axis, the droplet velocity shows a trend of gradually decreasing from the middle to the sides. The droplet size in the horizontal direction at the same height shows a gradual increase from a small droplet diameter in the middle to the sides, there are differences between the numerical simulation results of hedge nozzles and conventional fan nozzles.

Test verification

Testing was conducted with clean water under room temperature and windless indoor conditions, using a test system to perform nozzle atomisation (Figure 7) at pressures of 0.3, 0.5 and 0.7 MPa, the pressure droplet particle size of the hedge nozzle spray field was tested, see Figure 5.

FIGURE 7. Test system for atomisation performance of the nozzle.

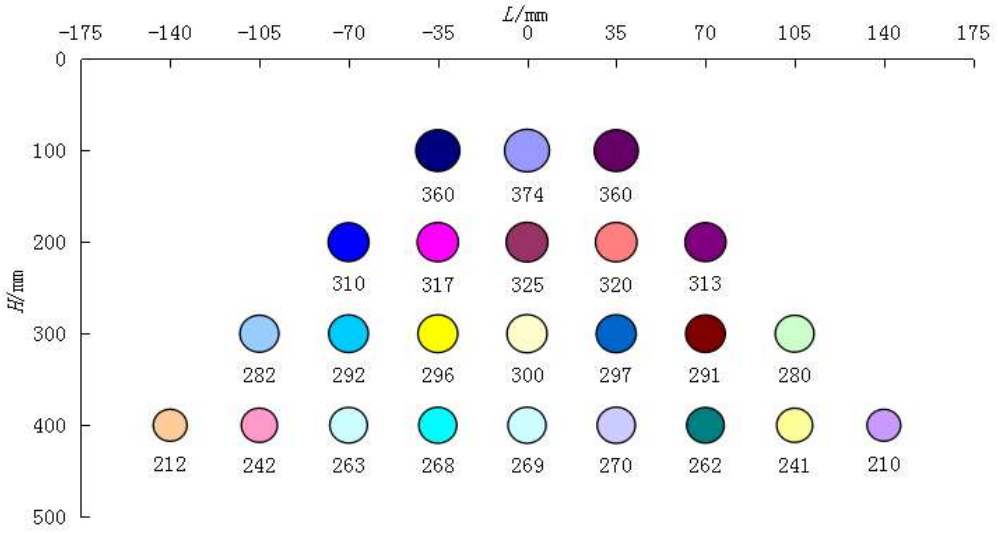

(a) 0.3 MPa

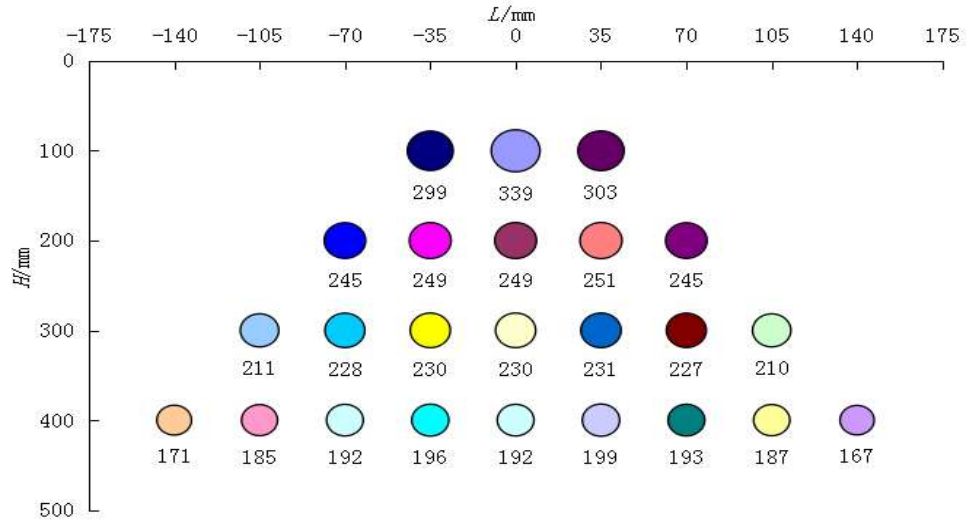

(b) 0.5 MPa

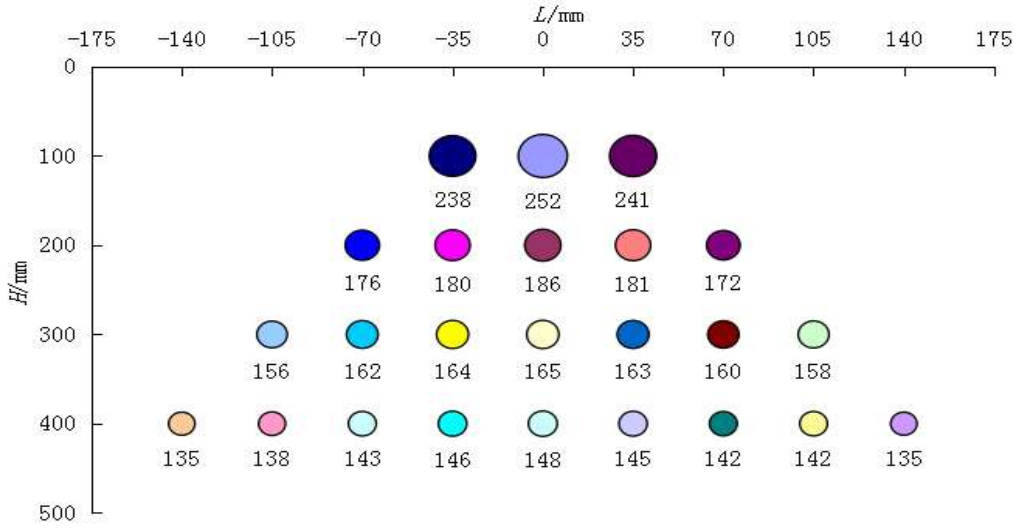

(c) 0.7 MPa

FIGURE 8. Particle size distribution of impingement nozzle.

Figure 8 shows that the spray pressure varies in the range 0.3-0.7 MPa and the droplet size gradually becomes smaller as the spray pressure increases in the positive direction along the axis (vertically downward), i.e. the test surface at 100, 200, 300, and 400 mm from the nozzle outlet. If the spraying pressure is 0.7 MPa, the droplet size will change from 252 μm to 148 μm. At the same level, the droplet size is larger and uniform in the middle but smaller on the two outermost sides. With the increase in spraying pressure, the droplet size at the test points on both sides will be close to the droplet size in the middle area. If the spraying pressure is 0.5 MPa on the 300 mm test surface, the droplet size between -70 mm and 70 mm is 227-231 μm. The droplet diameter at the edge of the spray fan, 105 mm away from the axis, is 210-211 μm. When the spraying pressure increases to 0.7 MPa, the droplet size between -140 mm and 140 mm is 156-165 μm, the variation range being only 9 μm. With the increase in spraying pressure, the spray amplitude of the fan-shaped surface will slightly increase but the droplet size will generally tend to be consistent at the same level. With the increase in spraying pressure, the droplets in the spray field tend to be homogenised. For example, when the spraying pressure is 0.7 MPa, at 200 mm and 400 mm horizontal heights, the droplet size tends to be close to the droplet size at 300 mm.

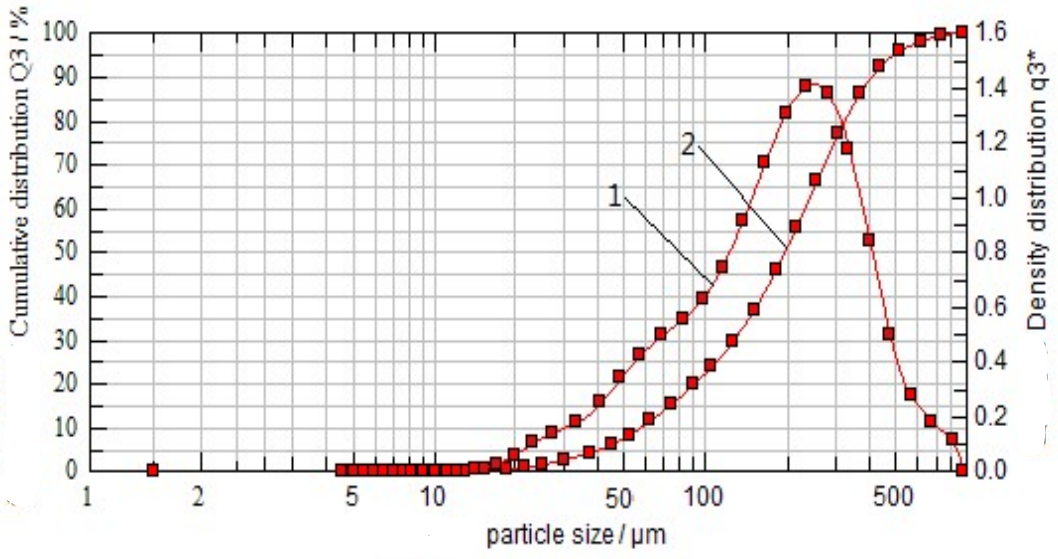

(a) flat-fan nozzle

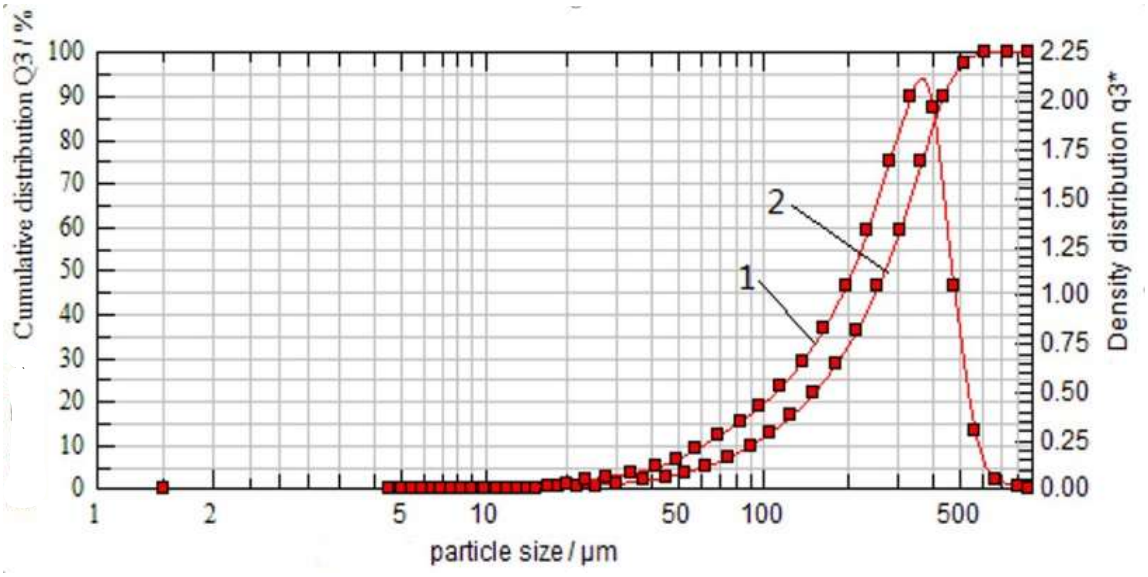

1-frequency distribution 2-cumulative distribution

(b) impingement nozzle

FIGURE 9. Droplet distribution.

The droplet distribution for the sector nozzle and impingement nozzle, measured under the same spraying pressure (0.5 MPa), is shown in Figure 9. Curves 1 and 2 represent the frequency distribution curve and cumulative distribution curve, respectively. It is obvious from the figure that the frequency distribution of the spray droplets of the fan nozzle is wide and presents a normal distribution, while the frequency distribution of the spray droplets of the impingement nozzle is narrow, which indicates that the distribution of the spray droplets is relatively concentrated and the spectrum of the spray droplets is narrow. This is because the two jets produce intense momentum transfer on the impact surface, leading to drastic changes in energy. Collision, extrusion and shearing may occur between flow clusters, causing them to deform and split. The impact makes the large fog droplets break and the smaller fog droplets combine to form larger fog droplets. In general, the droplet size tends to be uniform, reaching homogenisation. The greater the spraying pressure and the more intense the impact, the more obvious the droplet size homogenisation.

CONCLUSIONS

- After the impact of the two jets, with the increase of pressure, the splitting and uniformity of the liquid flow cluster improves. This is conducive to a smaller and more uniform droplet size at the impingement nozzle, a more concentrated droplet distribution, and the formation of a narrow droplet spectrum.
- The velocity component of the droplet in the vertical downward direction (z-axis) of the opposing jet nozzle, after the impact of the jet, is close to the same horizontal height (for example, the velocity component of the droplet is 70.33-73.70 m/s on the horizontal test surface 23 mm from the bottom of the nozzle body under a pressure of 0.5 MPa, and decreases along the positive axis direction. The velocity component of the droplet in the horizontal direction (x-axis) is small in the middle and large on both sides, and the velocity near the central axis is small and moves in an irregular direction. The velocity component of droplets in the front and rear directions (y-axis) is very small. Due to the close velocity component of the droplet velocity in the positive direction of the z-axis and the jet impact, the droplet group size will be homogenised, which is conducive to generating droplets with uniform size at the same level in the spray field. The velocity component of the droplet velocity in the x-axis direction has an effect on the spray amplitude of the nozzle.
- The droplet size on the fan shaped surface of the opposing jet spray nozzle is larger in the middle and uniform, but smaller on both sides. For example, the droplet size in the middle is 227-231 μm when the spraying pressure is 0.5 MPa on the test surface, at a horizontal height of 300 mm. The droplet size near the edge is 210-211 μm. This characteristic is beneficial to solve the problem of uneven droplet size distribution when the spray bar operates in the field. The experimental results are in agreement with the numerical simulation and theoretical analysis results.

REFERENCES

Cai Y, Duan Z, Niu J, Li D, Zhang J, Qiao G (2022) Numerical simulation of flow field characteristics in impinging stream continuous crystallizer. Chemical Engineering (China) 50(11):43-49.

Dong F, Zhou H, Shi M, Ru Y, Yi K (2019) Design and Atomisation Test of Impinging nozzle. Scientia Silvae Sinicae 55(1): 83-90.

Dong F, Zhou H (2018) Development of foreign plant protection nozzles. Acta Agriculturae Universitatis Jiangxiensis 40(4):866-874.

Dong F, Zhou H, Ru Y Shi M, Chen Q, Yi K (2018) Experiment on droplet distribution characteristics in spray field of impinging nozzle. Transactions of the Chinese Society for Agricultural Machinery 49(12):116-121+128.

Fei J, Sun F, Yang W, Fu Y, Wang Y (2015) Experimental analysis on movement and size distribution of atomised droplets from impinging liquid jet. Journal of Rocket Propulsion 41(1):10-14.

Gu Z, Zhao W, Zhang Y, Wei H (2015) A Research on the effects of mesh quality evaluation criteria on the results of vehicle external flow field simulation[J]. Automotive Engineering 37(11):1265-1269.

He X (2019) Research and development of crop protection machinery and chemical application technology in china. Chinese Journal of Pesticide Science. 21(5):921-930.

Lü X, He X, Song J, Zeng A, Andreas H (2007) Analysis of spray process produced by agriculture flat-fan nozzles. Transactions of the Chinese Society of Agricultural Engineering 23(9):95-100.

Salcedo R, Ramon L, Jordi C, Javier C, Michael G, Montserrat O, Paula G, Emi L (2020) Evaluation of leaf deposit quality between electrostatic and conventional multi-row sprayers in a trellised vineyard. Crop Protection 127:104964.

Song S, Chen J, Hong T, Xue X, Xia H, Song Y (2017) Variation of droplet diameter in wind field for long-range air-assisted sprayer. Transactions of the Chinese Society of Agricultural Engineering 33(6):59-66.

Wang G (2019) Spraying Quality Evaluation on Plant Protection UAV. Guangzhou: South China Agricultural University. 2019.6.

Wang X, Liu J, Zhang Q (2022) Water–Pesticide Integrated Micro-Sprinkler Design and Influence of Key Structural Parameters on Performance. Agriculture 12(10):1532.

Zhang J, Zhang Z, Feng Y, Dong X (2022) Advances in multiscale analysis of impinging streams flow field and mixing characteristics. Journal of Engineering Thermophysics 43(11):2944-2956.

Zheng G, Nie W, He B, Xue C (2015) Study on the influence of impact angle on the atomisation characteristics of impinging nozzle. Journal of Propulsion Technology 36(4):608-613.